Journal of Crystal Growth 310 (2008) 2774–2779

Contents lists available at ScienceDirect

Journal of Crystal Growth

journal homepage: www.elsevier.com/locate/jcrysgro

# Distribution of oxidation states of Cr ions in Ca or Ca/Mg co-doped Cr:$Y_3Al_5O_{12}$ single-crystal fibers with nitrogen or oxygen annealing environments

Cheng-Nan Tsai [a], Kuang-Yao Huang [a], Hann-Jong Tsai [a], Jian-Cheng Chen [a], Yen-Sheng Lin [b], Sheng-Lung Huang [c,*], Yen-Sheng Lin [d]

[a] Institute of Electro-Optical Engineering, National Sun Yat-Sen University, Kaohsiung 804, Taiwan
[b] Institute of Photonics and Optoelectronics, National Taiwan University, Taipei 106, Taiwan
[c] Institute of Photonics and Optoelectronics and Department of Electrical Engineering, National Taiwan University, Taipei 106, Taiwan
[d] Department of Electronic Engineering, I-Shou University, Kaohsiung 840, Taiwan

ARTICLE INFO

*Article history:*
Received 22 November 2007
Accepted 14 February 2008
Communicated by R.S. Feigelson
Available online 2 March 2008

*PACS:*
42.62.Fi
42.70.Hj
42.72.Ai
71.70.Ch

*Keywords:*
A1. Doping
A1. Optical microscopy
A2. Laser heated pedestal growth

ABSTRACT

The valence states of Cr ions in Ca or Ca/Mg co-doped Cr:$Y_3Al_5O_{12}$ (YAG) single-crystal fibers are studied. The fibers were grown using the laser-heated pedestal growth method, followed by annealing treatments up to 1500 °C. The concentrations of the $Cr^{3+}$ and $Cr^{4+}$ ions in octahedral and tetrahedral sites in oxygen or nitrogen environments were characterized. Above 700 °C, migration of $Cr^{4+}$ between octahedral and tetrahedral sites takes place; its relative stabilization energy was estimated. For Ca,Cr:YAG annealed in an oxygen or nitrogen environment, it was 0.25 and 0.3 eV, respectively. For Mg,Ca,Cr:YAG annealed in oxygen or nitrogen, it was 0.47 and 0.49 eV, respectively. For the Ca,Cr:YAG crystal fiber (Ca/Cr = 113.1%) with oxygen annealing, about 35% and 2.5% of Ca ions took part in charge compensation for $Cr^{4+}$ in the octahedral and tetrahedral sites, respectively. The density of oxygen vacancies depends on the concentration of Ca ions. The estimated ratios of the unreacted oxygen vacancies to total oxygen vacancies were about 63% and 88% for oxygen and nitrogen annealing, respectively. The main limitation on the concentration of $Cr^{4+}$ in the tetrahedral site of YAG is the presence of unreacted oxygen vacancies.



## 1. Introduction

There has been intense interest in the spectroscopy of $Cr^{4+}$ in tetrahedrally coordinated environments since room-temperature laser operation of Cr:$Y_3Al_5O_{12}$ (YAG) was demonstrated [1]. $Cr^{4+}$:YAG emission is in the near-infrared (NIR) from 1.2 to 1.6 μm, and may have applications in tunable and mode-locked solid-state lasers [2–6] and as super-broadband amplified spontaneous emission (ASE) in optical fiber communications [7,8]. When Cr and divalent ions (Ca, Mg) are introduced into YAG, there exist several Cr ion valence states. $Cr^{3+}$ is the dominant species, one which is rarely found in tetrahedrally coordinated sites [7,9] and this is substituted into the octahedral Al site, denoted as $Cr^{3+}_{oct}$. It is the most stable valence state of the Cr ion, and its crystal field stabilization energy is the largest. At high-temperature oxygen atmosphere with charge compensator, the $Cr^{4+}$ tends to be substituted into the tetrahedral Al site, and is denoted as $Cr^{4+}_{tetr}$ [10–13]. The garnets co-activated with chromium and divalent ions were shown to have $Cr^{4+}$ ions present both in tetrahedral and in octahedral positions [14]. It was found that irradiation of crystals prepared under reducing conditions forms color centers, with $Cr^{4+}$ ions in octahedral positions ($Cr^{4+}_{oct}$) having absorption in the UV and visible wavelength range. Oxidization and annealing form centers with $Cr^{4+}$ at tetrahedral sites, which show strong absorption in 1–1.2 μm wavelength range [15]. It was shown that the electronic recharging and charging processes $Cr^{4+}_{oct} \leftrightarrow Cr^{3+}_{oct}$ taking place in the octahedral sites of the garnet lattice have lower activation energies compared to the chromium migration process $Cr^{4+}_{tetr} \leftrightarrow Cr^{4+}_{oct}$ taking place at higher temperatures or with longer exposures [16]. The ratio $Cr^{4+}_{tetr}/Cr^{4+}_{oct}$ is about 4% at 1700 K and the relative stabilization energy $E_{CrAl}$ was found to be 0.11 eV [17]. Oxygen vacancies can also contribute to the charge compensation [13,18,19]. It is desirable to develop crystal-growth techniques to obtain high concentrations of these lasing centers.

The laser-heated pedestal growth (LHPG) method is fast, economical, flexible, and provides easy adjustment of growth conditions and dopant concentrations. It has been developed to pull $Cr^{4+}$:YAG crystal fibers to be used for generating several

* Corresponding author. Tel.: +886 2 33663700x348; fax: +886 2 33663692.
*E-mail address:* slhuang@cc.ee.ntu.edu.tw (S.-L. Huang).

0022-0248/$ - see front matter © 2008 Elsevier B.V. All rights reserved.
doi:10.1016/j.jcrysgro.2008.02.028

milli-watts of amplified spontaneous emission [7]. In this paper, using an electron gun to deposit MgO on the outside of the Ca,Cr:YAG crystal fiber and with post-growth oxygen and nitrogen annealing treatments, we have characterized the concentrations of Cr in various oxidation states, and analyzed Cr valence changes. The relative stabilization energy for the transformation from $Cr^{4+}_{oct}$ to $Cr^{4+}_{tetr}$ as well as the relationship between the concentrations of the charge compensators ($Ca^{2+}$, $Mg^{2+}$), $Cr^{3+}_{oct}$, $Cr^{4+}_{oct}$, $Cr^{4+}_{tetr}$, oxygen vacancies and total Cr have been determined. The efficiency of charge compensation is also analyzed. This paper presents, for the first time, a detailed and quantitative analysis of the $Cr^{4+}$ charge compensation efficiency with divalent co-doping.

## 2. Experimental procedure

### 2.1. Sample preparation

The Ca,Cr:YAG crystal fibers were prepared by the LHPG method. The source rods were Ca co-doped Cr:YAG with cross section 500 μm × 500 μm and crystal orientation 〈111〉. They were first grown at a speed of 24 mm/min with a $CO_2$ laser power of 6.5 W to create fibers of 290 μm in diameter. After cutting into 4 cm long pieces, they were placed in an electron gun chamber with an axially rotated mount for side deposition. The chamber temperature was set to 300 °C and the electron gun voltage to 6.5 kV. MgO was then deposited on the circumference of the Ca,Cr:YAG crystal fiber. After side deposition, the Cr:YAG crystal fibers ions co-doped with divalent ions were re-grown with 1.1-W $CO_2$ laser power at a speed of 2 mm/min to produce 70 μm diameter crystal fibers. Post-growth thermal annealing was performed at various temperatures in 1 atm of oxygen or nitrogen for 4 h.

### 2.2. Composition and fluorescence measurements

The composition of the crystal fibers was measured by an electron probe micro-analyzer (EPMA, JEOL JXA-8900R). The composition and doping profiles were scanned across the fiber cross-section. The concentrations of $Ca^{2+}$ and Cr ions in the Ca,Cr:YAG fiber were $1.68\times10^{19}$ and $1.49\times10^{19}$ ♯/cm$^3$ while [$Ca^{2+}$+$Mg^{2+}$] and Cr in the Mg,Ca,Cr:YAG fiber were $3.91\times10^{19}$ and $1.55\times10^{19}$ ♯/cm$^3$, respectively. The concentrations of $Ca^{2+}$ and Cr ions had contrasting distribution profiles as depicted in Fig. 1(a). It has been shown that both $Ca^{2+}$ and $Mg^{2+}$ accumulate near the fiber center, while the concentration of Cr ions is lower at the fiber center compared to the fiber perimeter [18]. The underlining physics is related to the segregation coefficients of $Ca^{2+}$, $Mg^{2+}$ and $Cr^{3+}$ in YAG crystals.

The EPMA measurement, however, cannot distinguish the oxidation states. Laser scanning confocal microscopy (LSCM) was employed to identify $Cr^{3+}_{oct}$ and $Cr^{4+}_{tetr}$ ions, by excitation with a 532 nm frequency doubled Nd:YAG laser and a 1064 nm Yb-doped fiber laser, respectively. An objective lens with a numerical aperture of 0.65 was employed to achieve a spatial resolution of about 1 μm. Fig. 1(b) shows the fluorescence mapping of a 920 μm diameter Cr:YAG fiber, which was used as a calibration standard for the $Cr^{3+}$ concentration from fluorescence measurements.

## 3. Results

### 3.1. $Cr^{3+}_{oct}$ and $Cr^{4+}_{tetr}$ fluorescence spectra

The emissions from $Cr^{3+}_{oct}$ and $Cr^{4+}_{tetr}$ are in the visible and NIR, respectively. With confocal fluorescence microscopy they can be distinguished with micron-level spatial resolution. Fig. 2(a) shows

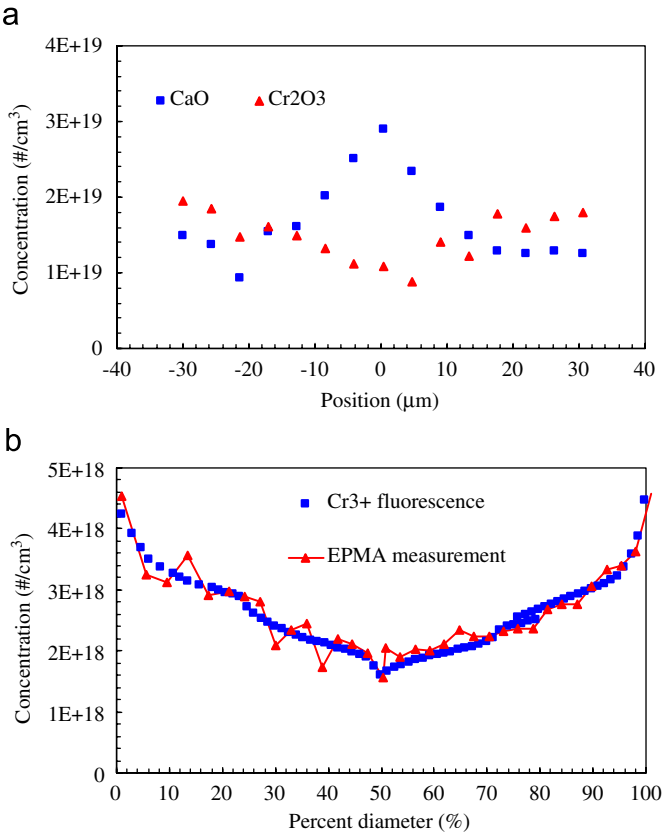


**Fig. 1.** (a) EPMA measured dopant profiles of a 70 μm Ca,Cr:YAG fiber. (b) Quantitative comparison between the LSCM and EPMA measurements.

the $Cr^{3+}_{oct}$ reflection fluorescence intensities showing the typical $Cr^{3+}_{oct}$ emission spectra from a sharp R-line (689 nm from $^2E\rightarrow{}^4A_2$ transition) [20–23] associated with three phonon sidebands (675, 707, and 726 nm). It was observed that the $Cr^{3+}_{oct}$ fluorescence intensity increases after oxygen annealing. The corresponding $Cr^{4+}_{tetr}$ fluorescence spectra are shown in Fig. 2(b). These spectra show the representative broadband emission from 1.2 to 1.6 μm resulting from the $^3T_2\rightarrow{}^3A_2$ transition. The central wavelength is at 1.38 μm with a 3 dB bandwidth of 265 nm. The $Cr^{4+}_{tetr}$ spectral density of the as-grown samples also increases with oxygen annealing.

### 3.2. The influence of nitrogen and oxygen annealing treatments

The Ca,Cr:YAG and Mg,Ca,Cr:YAG single-crystal fibers were annealed in a nitrogen or oxygen atmosphere at different temperatures and then the fluorescence intensities of $Cr^{3+}_{oct}$ and $Cr^{4+}_{tetr}$ were measured. In Figs. 3(a) and 4(a), a critical temperature can be seen at about 700 °C. With oxygen annealing, chromium migration takes place from the octahedral site to the tetrahedral site at higher temperatures, which promotes the $Cr^{4+}_{tetr}$ fluorescence intensity. The chromium migration proceeds in the opposite direction with nitrogen annealing, $Cr^{4+}_{tetr}\rightarrow Cr^{4+}_{oct}$[15–17], which decreases the $Cr^{4+}_{tetr}$ fluorescence intensity. In contrast to $Cr^{4+}_{tetr}$, the fluorescence intensity of $Cr^{3+}_{oct}$, as shown in Figs. 3(b) and 4(b), is greater with a nitrogen atmosphere than with an oxygen atmosphere. This is due to more $Cr^{3+}_{oct}$ ions being transformed into $Cr^{4+}$ ions with oxygen annealing. The $Cr^{3+}_{oct}$ is partially oxidized during fiber growth, and is stabilized as $Cr^{4+}_{tetr}$ in a distorted tetrahedral coordination. When the annealing temperature increases from 25 to 700 °C, the $Cr^{4+}_{tetr}$ fluorescence intensity

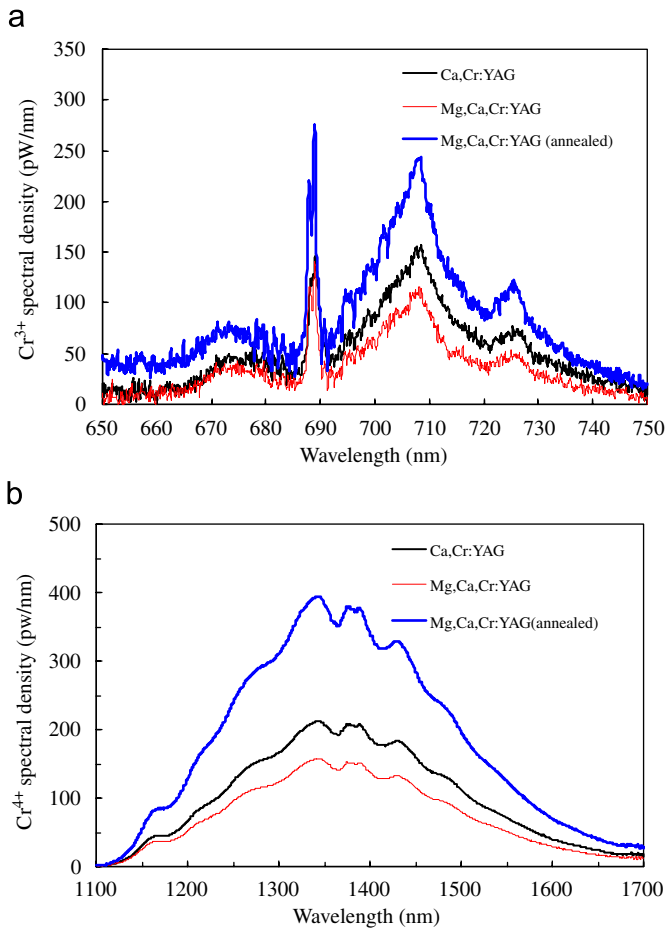


**Fig. 2.** The reflected fluorescent spectra of (a) $Cr^{3+}_{oct}$ and (b) $Cr^{4+}_{tetr}$ from Ca,Cr:YAG, and Mg,Ca,Cr:YAG as-grown samples, and Mg,Ca,Cr:YAG after oxygen annealing at 1350 °C.

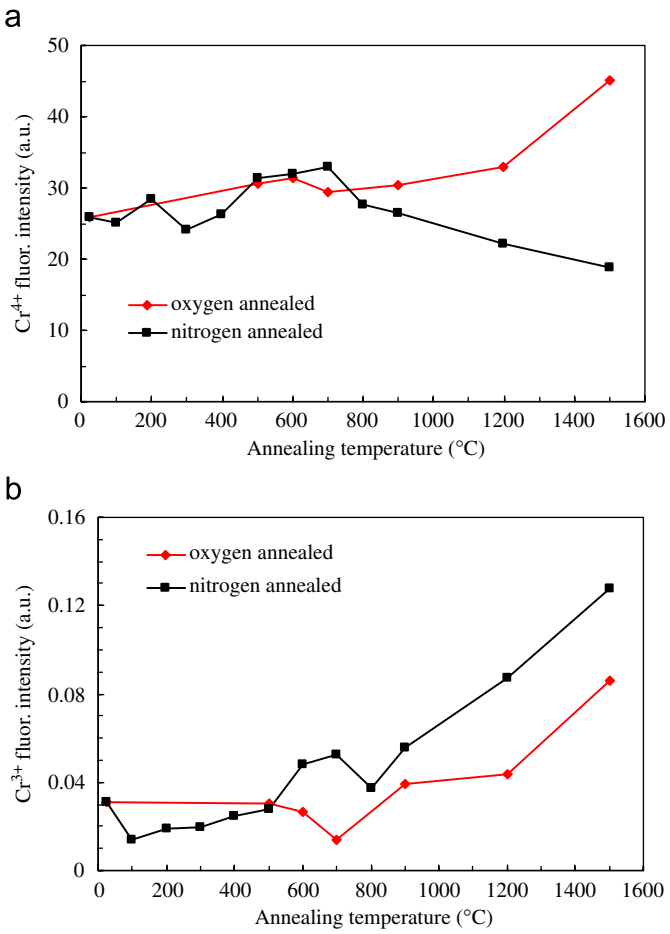


**Fig. 3.** (a) $Cr^{4+}_{tetr}$ and (b) $Cr^{3+}_{oct}$ fluorescence intensities for Ca,Cr:YAG single-crystal fibers with nitrogen and oxygen annealing.

increases slightly with the nitrogen and oxygen annealing as shown in Figs. 3(a) and 4(a). As depicted in Figs. 3(b) and Fig. 4(b), there are many $Cr^{3+}_{oct}$ ions doped into distorted octahedral sites.

The experimental result can be summarized as follows. There are two major conditions that affect the fluorescence intensity: one is the lattice quality of the Cr:YAG crystal, which depends on the annealing temperature; the other is the basic reaction of the Cr valence change. The greater the concentration of divalent co-doped ions the greater is the distortion of the lattice coordination. The $Cr^{4+}_{tetr}$ and $Cr^{3+}_{oct}$ fluorescence intensities of the Mg,Ca,Cr:YAG samples were lower than that of the Ca,Cr:YAG sample at 25 °C because of the increased number of defects. With a higher annealing temperature, the lattice quality and redox equilibrium changes significantly between 700 and 1500 °C. At an annealing temperature of 1500 °C, we obtained the highest fluorescence efficiency. So the following concentration analyses were performed at this annealing temperature.

## 4. Discussion and analysis

### 4.1. Analysis of chromium ion states and the relative stabilizing energy

YAG has a cubic crystal structure (space group Ia3d) with eight formula units per unit cell. The 24 Y atoms of the unit cell are surrounded by a dodecahedron of O atoms, while 16 (40%) of the Al atoms are surrounded by oxygen octahedra and 24 (60%) of the Al atoms are surrounded by oxygen tetrahedra [10]. Assuming that no ions occupy interstitial lattice positions when divalent metal oxides are doped into the YAG matrix, the following formula satisfies charge neutrality [13]:

$$2MeO + 2X^{3+} + O^{2-} \leftrightarrow 2Me^{2+} + V_o^{2+} + X_2O_3. \quad (1)$$

$Al^{3+}$ and $Y^{3+}$ ions are denoted as $X^{3+}$, the oxygen vacancy is denoted as $V_o^{2+}$, Ca and Mg are denoted as Me.

The chromium ions in the YAG crystal substitute aluminum ions and normally occupy octahedral sites, giving $Cr^{3+}_{oct}$ emission [11]. The $Cr^{3+}_{oct}$ can change its oxidation state to 4 with the help of Me ions, which serve as charge compensators as shown below [11,13,24]:

$$Cr^{3+}_{oct} + \tfrac{1}{2}(V_o^{2+} + 2Me^{2+}) + \tfrac{1}{4}O_2 \leftrightarrow (Cr^{4+}_{oct} + Me^{2+}). \quad (2)$$

The oxygen vacancies exist in co-doped garnet as complexes ($V_o^{2+}$+$2Me^{2+}$).

During annealing, oxygen vacancies diffuse and recombine with atmospheric oxygen at the surface of the crystal fiber. A positive charge thus released is transported by the hole to the crystal's volume, located on a $Cr^{3+}_{oct}$ in an octahedral site and a $Cr^{4+}_{oct}$ ion is formed. For the reverse direction of the equation, the positive charge is transported from the $Cr^{4+}_{oct}$ ion to the crystal's surface and the opposite conversion takes place [17]. At high temperatures, the chromium ions migrate toward the tetrahedral

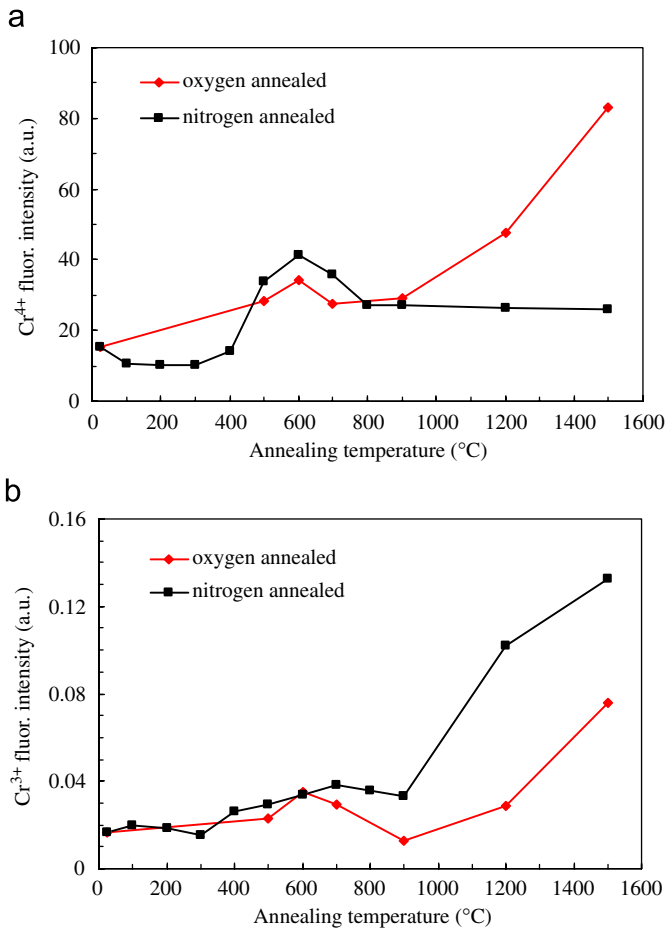


**Fig. 4.** (a) $Cr^{4+}_{tetr}$ and (b) $Cr^{3+}_{oct}$ fluorescence intensities for Mg,Ca,Cr:YAG single-crystal fibers with nitrogen and oxygen annealing.

sites and the reaction is [17,24]

$$Cr^{4+}_{oct} + Al^{3+}_{tetr} \leftrightarrow Cr^{4+}_{tetr} + Al^{3+}_{oct}. \quad (3)$$

Application of the mass action law to reaction (3) leads to the relationship [17,25]

$$\frac{[Cr^{4+}_{tetr}]}{[Cr^{4+}_{oct}]} = K_0 e^{-E_{CrAl}/k_B T}. \quad (4)$$

The relative stabilization energy of the reaction is $E_{CrAl}$. $k_B$ is Boltzman's constant. $T$ is the temperature (in Kelvin). Bracketed species stand for the appropriate ion concentration. The equations above are the basic reactions in the co-doped YAG. According to Eqs. (1) and (2), the incorporated divalent ions generates oxygen voids, and some of the oxygen voids react with $Cr^{3+}_{oct}$ to produce $Cr^{4+}$. This can be quantified as

$$2[Me^{2+}] = [V_0^{2+}] + 2[Cr^{4+}_{oct}] + 2[Cr^{4+}_{tetr}]. \quad (5)$$

Firstly, the mole percentage of the divalent ions to that of Cr is less than 2.5 in this work, and the $Cr^{4+}_{tetr}$ fluorescence intensity is greatly increased after oxygen annealing. Secondly, the radius of $Cr^{4+}_{tetr}$ is about 55 pm, which is much smaller than that of $Cr^{6+}_{tetr}$(69 pm). Therefore, it is reasonable to expect negligible quantities of $Cr^{6+}_{tetr}$ [10,19,24]. Our defect study on the Cr:YAG crystal fibers has shown that the defect densities are usually very low, i.e. less than $2.6 \times 10^{-6}$ ♯/cm$^2$. Therefore, interstitial defects can be neglected in our samples, and the conservation of chromium ions can be expressed as

$$[Cr] = [Cr^{3+}_{oct}] + [Cr^{4+}_{oct}] + [Cr^{4+}_{tetr}]. \quad (6)$$

The concentrations of Cr, $Ca^{2+}$, and $Mg^{2+}$ were measured by EPMA. $Cr^{3+}_{oct}$ and $Cr^{4+}_{tetr}$ were derived from the fluorescence measurements. Combining Eqs. (4–6), the concentrations of $Cr^{4+}_{oct}$, non-reacted $V_o^{2+}$, and the relative stabilization energy $E_{CrAl}$ were obtained.

As mentioned earlier, we analyzed the experimental data at 1500 °C. The measured $Cr^{3+}_{oct}$ fluorescence intensity with oxygen annealing at 1500 °C was calibrated by an EPMA measurement. The $Cr^{4+}_{tetr}$ fluorescence intensity was calibrated by its absorption coefficient and compared with the results of Sugimoto and Borodin [11,26] to estimate the $Cr^{4+}_{tetr}$ concentration. The $Cr^{4+}_{tetr}$ fluorescence intensity has been converted into the $Cr^{4+}_{tetr}$ concentration by adopting the absorption cross-section of $5 \times 10^{-18}$ cm$^2$ [18]. Lipavsky et al. [27] showed that there is no significant impact of the co-dopants ($Mg^{2+}$ or $Ca^{2+}$) on the optical absorption of the

**Table 1**
The ratio of the concentrations of divalent dopant (Me), $Cr^{3+}_{oct}$, $Cr^{4+}_{oct}$, $Cr^{4+}_{tetr}$ ions to the total Cr ions, and the relative stabilizing energy ($E_{CrAl}$) for Ca,Cr:YAG (sample ♯1) and Mg,Ca,Cr:YAG (sample ♯2) single-crystal fibers

| Sample no. | Annealing environment | Me/Cr (%) | $Cr^{3+}_{oct}$/Cr (%) | $Cr^{4+}_{oct}$/Cr (%) | $Cr^{4+}_{tetr}$/Cr (%) | $E_{CrAl}$ (eV) |
|---|---|---|---|---|---|---|
| 1 | $O_2$ | 113.1 | 57.8 | 39.4 | 2.8 | 0.25 |
| 1 | $N_2$ | 113.1 | 85.5 | 13.3 | 1.2 | 0.30 |
| 2 | $O_2$ | 252.3 | 48.9 | 46.1 | 5.0 | 0.47 |
| 2 | $N_2$ | 252.3 | 85.2 | 13.2 | 1.6 | 0.49 |

The annealing temperature was 1500 °C at 1 atm.

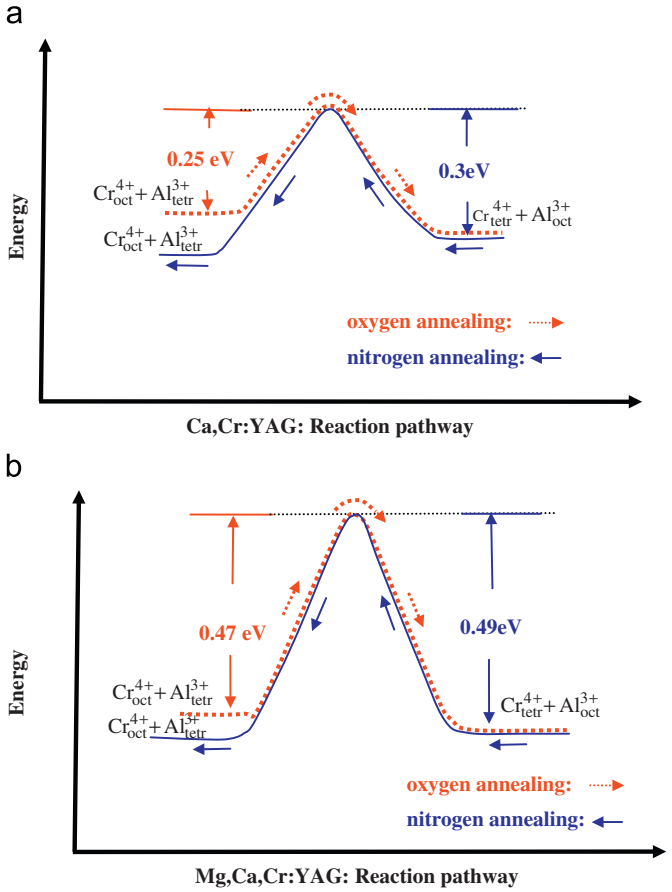


**Fig. 5.** The relative stabiliziation energies of (a) Ca,Cr:YAG, and (b) Mg,Ca,Cr:YAG single-crystal fibers with oxygen and nitrogen annealing.

**Table 2**
The percentages of $Cr^{4+}_{tetr}$ and $Cr^{4+}_{oct}$ relative to the divalent dopants and total Cr ions, and the percentage of non-reaction oxygen vacancies relative to the total oxygen vacancies

| Sample no. | Annealing environment | $Cr^{4+}_{tetr}/Mg^{2+}+Ca^{2+}$ (%) | $Cr^{4+}_{oct}/Mg^{2+}+Ca^{2+}$ (%) | Non-reaction $V_o^{2+}$/total $V_o^{2+}$ (%) | $Cr^{4+}_{tetr}+Cr^{4+}_{oct}+Cr$ (%) |
|---|---|---|---|---|---|
| 1 | $O_2$ | 2.5 | 34.8 | 62.7 | 42.2 |
| 1 | $N_2$ | 1.0 | 11.8 | 87.2 | 14.5 |
| 2 | $O_2$ | 2.0 | 18.2 | 79.8 | 51.5 |
| 2 | $N_2$ | 0.6 | 5.2 | 94.2 | 14.8 |

$Cr^{4+}$ ion in YAG, at least at 1064 nm. Therefore, the $Cr^{3+}_{oct}$ concentrations of Ca,Cr:YAG samples with oxygen and nitrogen annealing at 1500 °C were determined to be $8.58\times10^{18}$ and $1.27\times10^{19}$ ♯/cm$^3$, respectively. Similarly in the Mg,Ca,Cr:YAG samples, they were $7.58\times10^{18}$ and $1.32\times10^{19}$ ♯/cm$^3$, respectively. The $Cr^{4+}_{tetr}$ concentration in the Ca,Cr:YAG samples in oxygen and nitrogen at 1500 °C were $4.17\times10^{17}$ and $1.75\times10^{17}$ ♯/cm$^3$, and they were $7.68\times10^{17}$ and $2.4\times10^{17}$ ♯/cm$^3$ in the Mg,Ca,Cr:YAG samples. Table 1 summarizes the results of annealing at 1500 °C. For sample ♯1, i.e. the Ca,Cr:YAG crystal, with oxygen annealing, the ratios of $Cr^{3+}_{oct}$/Cr, $Cr^{4+}_{oct}$/Cr, and $Cr^{4+}_{tetr}$/Cr were 57.8%, 39.4%, and 2.8%, respectively. In view of Fig. 3, the evolution of the Cr valence and migration follow the path $Cr^{3+}_{oct}\rightarrow Cr^{4+}_{oct}\rightarrow Cr^{4+}_{tetr}$. In contrast, with nitrogen annealing, the evolution of the Cr valence and migration follows a reverse path, i.e. $Cr^{4+}_{tetr}\rightarrow Cr^{4+}_{oct}\rightarrow Cr^{3+}_{oct}$. There were similar results for sample ♯2. It was observed that the higher the concentration of divalent dopant ions, the larger the percentage of $Cr^{4+}_{tetr}$ arising with oxygen annealing.

The relative stabilization energy $E_{CrAl}$ in Table 1 was estimated using Eq. (4). For sample ♯1, $E_{CrAl}$ with oxygen annealing was about 0.25 eV, while with nitrogen annealing it was about 0.30 eV. For sample ♯2, these values were 0.47 and 0.49 eV for oxygen and nitrogen annealing, respectively. The reaction pathway can be depicted using Fig. 5. With either annealing, the Mg,Ca,Cr:YAG crystal fiber has a higher relative stabilization energy than the Ca,Cr:YAG crystal fiber. A probable reason is that there is a large misfit produced by the $Mg^{2+}$ in replacing the octahedral $Al^{3+}$ site, which causes excessive distortion in the YAG matrix. So the octahedrons were enlarged, thus increasing the stress, which, as a consequence, increases the relative stabilization energy.

### *4.2. Reduced charge compensation efficiency due to oxygen vacancies*

As shown in Eqs. (1) and (2), the doped divalent ions promote charge compensation as well as oxygen vacancies. The latter reduces the charge compensation efficiency. Based on the analysis in Section 4.1, the percentages of $Cr^{4+}_{tetr}$and $Cr^{4+}_{oct}$ to total Cr, and the percentage of un-reacted oxygen vacancies to the total oxygen vacancies are summarized in Table 2. For either oxygen or nitrogen annealing, less than 3% of the divalent dopant ions became active for charge compensation and produce $Cr^{4+}_{tetr}$ for NIR emission. For the Ca,Cr:YAG crystal fiber, there were 34.8% and 2.5% of $Ca^{2+}$ ions available to charge compensate and produce $Cr^{4+}$ in octahedral and tetrahedral sites with oxygen annealing. In the nitrogen atmosphere, only 11.8% and 1% of $Ca^{2+}$ were active. For the Mg,Ca,Cr:YAG crystal fiber, charge compensation for the divalent dopant ions was lower than that for the Ca,Cr:YAG crystal, but charge compensation for the Cr ions was higher. The ratio of un-reacted oxygen vacancies to the total oxygen vacancies was about 63% and 87% with oxygen and nitrogen annealing of the Ca,Cr:YAG crystal fiber. These values were 80% and 94% for the Mg,Ca,Cr:YAG crystal fiber. This result shows that the low charge compensation efficiency is mainly due to the existence of oxygen vacancies in the YAG matrix. The majority of the generated oxygen vacancies remained un-reacted.

## 5. Conclusion

The oxidation states of Cr ions in Cr:YAG crystal fibers co-doped with divalent ions have been studied quantitatively. There are two conditions that affect the chromium valence change in the YAG crystal fiber. One is the electronic charging and recharging process, $Cr^{4+}_{oct}\leftrightarrow Cr^{3+}_{oct}$, which depends on temperature, the concentration of divalent ions, the ambient atmosphere and the number of oxygen vacancies. The other is the chromium migration process, $Cr^{4+}_{tetr}\leftrightarrow Cr^{4+}_{oct}$, which depends on the annealing temperature. The relative stabilization energy of Cr ions between octahedral and tetrahedral sites is analyzed. The YAG fibers with $Mg^{2+}$ doping showed higher relative stabilization energy than those with $Ca^{2+}$. Oxygen annealing facilitates the $Cr^{3+}_{oct}\rightarrow Cr^{4+}_{oct}\rightarrow Cr^{4+}_{tetr}$ charge compensation and migration path. The migration of $Cr^{4+}_{oct}$ in the YAG lattice to $Cr^{4+}_{tetr}$ takes place above 700 °C. Oxygen vacancies are the major cause of the reduced charge compensation efficiency. For the Ca,Cr:YAG sample, up to 37.3% of the divalent ions compensated the $Cr^{3+}$ to $Cr^{4+}$, though only 2.5% was active in fluorescence. For the Mg,Ca,Cr:YAG crystal fiber, less than 2% of the divalent ions became active for charge compensation to $Cr^{4+}_{tetr}$. The ratio between un-reacted and total oxygen vacancies in the Ca,Cr:YAG fiber is smaller than that of the Mg,Ca,Cr:YAG fiber. The majority of the oxygen vacancies were un-reacted, which is the main reason why $Cr^{4+}_{tetr}$ concentrations are usually limited to less than 5% of the total Cr ions.

## Acknowledgments

The authors are grateful to Mr. B. Chiang for composition analysis using EPMA. The authors also gratefully acknowledge the support of this research by the Ministry of Education Program for Promoting Academic Excellence of Universities under grant number 91-E-FA08-1-4.

## References

[1] A. Sennaroglu, C.R. Pollock, H. Nathel, J. Opt. Soc. Am. B 12 (1995) 930.
[2] N.B. Angert, N.I. Borodin, V.M. Garmash, V.A. Zhitnyuk, A.G. Okhrimchuk, O.G. Siyuchenko, A.V. Shestakov, Sov. J. Quantum Electron. 18 (1988) 73.
[3] P.M.W. French, N.H. Rizvi, J.R. Talor, A.V. Shestakov, Opt. Lett. 18 (1993) 39.
[4] Y. Ishida, K. Naganuma, Opt. Lett. 21 (1996) 51.
[5] I.T. Sorokina, S. Naumov, E. Sorokin, E. Wintner, Opt. Lett. 24 (1999) 1578.
[6] T. Ishii, K. Fujimura, K. Ogasawara, H. Adachi, I. Tanaka, J. Phys. Condens. Matter 13 (2001) 5757.
[7] C.Y. Lo, K.Y. Huang, J.C. Chen, S.Y. Tu, S.L. Huang, Opt. Lett. 29 (2004) 439.
[8] C.Y. Lo, K.Y. Huang, J.C. Chen, C.Y. Chuang, C.C. Lai, S.L. Huang, Y.S. Lin, P.S. Yeh, Opt. Lett. 30 (2005) 129.
[9] C. Batchelor, W.J. Chung, S. Shen, A. Jha, Appl. Phys. Lett. 82 (2003) 4035.
[10] B.M. Tissue, W. Jia, L. Lu, W.M. Yen, J. Appl. Phys. 70 (1991) 3775.
[11] A. Sugimoto, Y. Nobe, K. Yamagishi, J. Crystal Growth 140 (1994) 349.

[12] S. Ishibashi, K. Naganuma, I. Yokohama, J. Crystal Growth 183 (1998) 614.
[13] S.A. Markgraf, M.F. Pangborn, R. Dieckmann, J. Crystal Growth 180 (1997) 81.
[14] L.I. Krutova, A.V. Lukin, V.A. Sandulenko, E.A. Sidorova, V.M. Solntsev, Opt. Spektrosk. 63 (1987) 1174
Opt. Spectrosc. (USSR) 63 (1987) 693.
[15] L.I. Krutova, N.A. Kulagin, V.A. Sandulenko, A.V. Sandulenko, Fiz. Tverd. Tela (Leningrad) 31 (1989) 170
Sov. Phys. Solid State 31 (1989) 1193.
[16] S.B. Ubizskii, S.S. Melnyk, B.V. Padlyak, A.O. Matkovskii, A. Jankowska-Frydel, Z. Frukacz, Proc. SPIE 4412 (2001) 63.
[17] A.G. Okhrimchuk, A.V. Shestakov, Opt. Mater. 3 (1994) 1.
[18] J.C. Chen, C.Y. Lo, K.Y. Huang, F.J. Kao, S.Y. Tu, S.L. Huang, J. Crystal Growth 274 (2005) 522.
[19] J.C. Chen, K.Y. Huang, C.N. Tsai, Y.S. Lin, C.C. Lai, G.Y. Liu, F.J. Kao, S.L. Huang, J. Appl. Phys. 99 (2006) 093113.
[20] A.L. Schawlow, J. Appl. Phys. 33 (1962) 395.
[21] P. Kisliuk, W.F. Krupke, J. Appl. Phys. 36 (1965) 1025.
[22] G. Dominiak-Dzik, W. Ryba-Romanowsk, M. Grinberg, E. Beregi, L. Kovacs, J. Phys. Condens. Matter 14 (2002) 5229.
[23] W.C. Zheng, J. Phys.: Condens. Matter 7 (1995) 8351.
[24] J. Dong, P. Deng, J. Xu, Opt. Commun. 170 (1999) 255.
[25] L. Schuh, R. Metselaar, G. de. With, J. Appl. Phys. 66 (1989) 2627.
[26] N.I. Borodin, V.A. Zhitrnyuk, A.G. Okhimchuk, A.V. Shestakov, Bull. Acad. Sci. USSR Phys. Ser. 54 (1990) 54.
[27] B. Lipavsky, Y. Kalisky, Z. Burshtein, Y. Shimony, S. Rotman, Opt. Mater. 13 (1999) 117.